Potentiality of new miniature-channels Stirling regenerator

Alfarawi, Suliman; Al-Dadah, Raya; Mahmoud, Saad

DOI:
10.1016/j.enconman.2016.12.017

Potentiality of new miniature-channels Stirling regenerator

S. Alfarawi[1,a], R. AL-Dadah[1], S. Mahmoud[1]

[1]*Department of Mechanical Engineering, University of Birmingham, Edgbaston, B15 2TT, UK*

[a]e-mail: ssa178@bham.ac.uk

Abstract

This paper deals with the development of new Stirling regenerator as one of parallel-geometry regenerators. Circular miniature-channels with different diameters, 1.5, 1.0, 0.6, 0.5, 0.4 (mm) were adopted for the current design. A 3D CFD approach, based on transient conjugate heat transfer was performed on a regenerator sector to obtain the fluid flow and heat transfer characteristics of each configuration. The obtained data was converted into an equivalent porous media to be utilized in a full CFD model of the engine developed by the author in other study. The results revealed that the 0.5mm channel regenerator had good potential close to random fibre regenerator for maximizing engine indicated power. However, engine performance was adversely affected by the excessive heat rejected from the cooler due to the inherit axial conduction loss of channel regenerators compared to conventional regenerator. The results also showed that the proper selection of matrix material with high volumetric heat capacity and low thermal conductivity can alleviate these losses and reduce the heat rejected from the engine. This study suggested further experimental work to investigate the effect of channel regenerator segmentations to minimize the axial conduction losses and improve the regenerator performance.

Keywords: Circular-shaped, Stirling regenerator, miniature-channels.

Nomenclature

A_f	Internal flow area (m^2)	Re	Reynolds number
C_p	Gas heat capacity at constant pressure (J/kg. K)	r_i	Sector inner radius (m)
D	Pipe diameter (m)	r_o	Sector outer radius (m)
D_h	Regenerator hydraulic diameter (m)	S	Fabrication clearance (m)
d_{ch}	Channel diameter (m)	T	Fluid temperature (K)
f	Darcy friction factor	T_m	Mean bulk fluid temperature (K)
h_x	Local heat transfer coefficient (W/m^2. K)	T_w	Wall temperature (K)
K	Permeability (m^2)	u	Fluid velocity (m/s)
k_f	Fluid thermal conductivity (W/m. K)	VSWE	Expansion swept volume (m^3)
k_s	Solid thermal conductivity (W/m. K)	***Greek letters***	
Nu	Average Nusselt number	β_F	Forchheimer drag coefficient, kg/m^4
P_r	Radial pitch (m)	δ	Thermal penetration depth (m)
$P_\emptyset$	Angular pitch (°)	ρ	Fluid density, kg/m^3
p	Fluid pressure (Pa)	μ	Fluid dynamic viscosity, Pa. s
$''q_x$	Local heat flux (W/m^2)	ε	Porosity

1. Introduction

The Stirling engine is an externally-heated engine, it is thermally regenerative, simple in construction, virtually quiet, safe in operation, and intrinsically flexible to adopt any heat source such as solar, biomass, geothermal energy or even an industrial waste [1]. However, its low specific power compared to internal combustions engines (ICE) and the highly initial cost of the engine may still hinder further development and optimization of Stirling machines. The successful development of an efficient and cost effective Stirling engine will have a significant impact on the recovery of the available waste heat sources leading to significant reduction in fossil fuel consumption and CO2 emissions.

The regenerator is a key component of the engine, it is an internal heat exchanger that acts as a thermal sponge when absorbing and releasing heat at a portion of the cycle, thus, engine power and efficiency are enhanced. The heat being absorbed and restored to the gas in the regenerator during one cycle is typically four times the heat that passes through the heater during one cycle [2]. For an engine without a regenerator, its heater would need to take in five times as much heat during a cycle as that with a regenerator to generate the same power.

Stirling engines mostly use wire mesh (woven or random fibre) as a conventional regenerator due to its high convective heat transfer between the solid and the gas resulting from the extended surface area of wires (this is similar to a cross flow over repeated cylinder-shaped wires), and low axial conduction in flow direction. However, the downside of this type of regenerators is the high flow friction resulting from flow separation, eddies associated with stagnation areas that can degrade the engine performance [3]. The regenerator has to have several features for better performance that might be contradicting and this pause a challenge for developers to find the optimum configuration that least fulfils the requirement of maximum convective heat transfer, minimum pressure drop, and minimum axial conduction in flow direction [4, 5].

Theoretically, a regenerator, with its heat transfer surfaces parallel to the oscillatory flow, has better performance than the conventional mesh regenerator type [6]**.** This type of regenerator has some interesting features in spite of the high heat transfer such as; (1) small frictional losses due to the minimum flow separation; (2) low dead volume

which means that they can be fabricated as compact as possible. However, the intrinsic axial conduction losses are large due to the continuity of solid material and this crucial disadvantage can degrade its performance.

The regenerator performance is often evaluated experimentally on a real engine test-stand or on a tailor-made test-stand based on unidirectional flow or oscillatory flow. However, in recent years, analytical, numerical models and the sophisticated CFD packages for Stirling engine analysis have emerged to shift from the tedious and expensive experimental work. In their hierarchal order, they are classified as zeroth, first, second, third and fourth order models [7]. These models are ascending in their complexity and accuracy however, the effects caused by the geometrical variation can only be handled by the adoption of fourth-order analysis or namely computational fluid dynamics (CFD). These models can be used to judge the regenerator performance through a full simulation of the engine or the regenerator alone.

There have been several studies on the conventional Stirling engine regenerators in literature. Martaj et al [8] presented an energetic, entropic and exegetic analysis of LTD gamma-type Stirling engine based on steady state operation. Using zero-dimensional numerical model, the engine was split into three isothermal control volumes, including the heater, cooler and regenerator. Energy, mass, entropy and exergy balance was carried out on each cell based as a function of crank angle (kinematics-thermodynamic coupling). Their results showed that it was possible to optimize engine components based on best efficiency and minimum production of entropy and that the regenerator's dead volume had strong impact on thermal and exergy efficiencies for the whole engine. Shendage et al [9] investigated the effect of geometrical dimensions of a regenerator on beta-type Stirling engine performance. They used a thermodynamic analysis based on second-order simulation to evaluate engine performance. Different losses were accounted for in the analysis including reheat, shuttle conduction, pumping and heat exchangers effectiveness. The number of wire sheets in the regenerator were varied depending on the pressure drop, dead volume and the thermal penetration depth. They proposed a length of the regenerator of 22 mm that balanced the conflicting increased heat transfer and pressure drop due to the increase in number of sheets which gave a regenerator an optimum effectiveness of 0.965. Mahkamov [10] performed a second-order and 3D CFD analysis on a gamma-type Stirling engine prototype to enhance its power. The CFD results revealed that power reduction was attributed to the high level of hydraulic losses in the regenerator, and the entrapment of the gas in the pipe

connecting the two parts of the compression space and to its large dead volume. A further improvement in the engine design was only viable by adopting this multi-dimension approach within an acceptable range of accuracy, 18% when compared to experimental results. Torre [11] developed a 2D CFD model for 300 cm^3 beta-type Stirling engine simulation based on OpenFoam code where turbulence effects and porous media modelling were considered. Parametric study was carried out to investigate the effects of charge pressure, heat input to the heater and regenerator material thermal conductivity on engine power. It was found that increasing both charge pressure and heat input increase engine power. Meanwhile, lower thermal conductivity material of the regenerator enhances the engine performance due the reduced axial conduction in the regenerator. It was reported that when using helium against air as working gas, no significant difference in power output was observed. Costa et al [12] developed a CFD model based on finite volume method (FVM) to derive Nusselt number correlations of two types of regenerator matrices; stacked and wound woven wires. The stacked woven wire correlation was first compared to an existing experimental correlation to validate the numerical method. Then, the correlation of for wound woven wire is proposed for investigated parameters of a diameter range from 0.08 to 0.11 mm and a porosity range from 0.60 to 0.68. Chen et al [13] constructed and tested a twin power piston gamma-type Stirling engine. The engine was incorporated with a moving regenerator housed inside its displacer and filled with a woven-screen material. The effects of different regenerator parameters on engine performance, including regenerator material, wire diameter, filling factor and stacking arrangements, were investigated. According to their results, copper material was found superior to stainless steel on engine performance at the tested conditions and optimum filling factor was proposed. Gheith et al [14] conducted an experimental investigation on the optimum regenerator matrix material and porosity for gamma-type Stirling engine. Different materials were tested including stainless steel, copper, aluminium and Monel 400. The results showed that stainless steel matrix with 85% porosity is the best configuration to maximize engine performance. Gheith [15] studied experimentally a new phenomenon associated with gamma-type Stirling engine causing a thermal energy dissipation in the regenerator. They observed that a maximum temperature of 25 ˚C between regenerator two sides can occur at heater temperature of 200 ˚C, the asymmetry of the engine and the one inlet of the cooling circuit causes this phenomenon. They carried out multi objective optimization to find the optimum operating values that minimizes this temperature difference in the regenerator and they found that heating temperature of 350 ˚C, initial pressure of 8 bar and cooling water flow rate 8.1 L/min can minimize this temperature difference to 17 ˚C.

As micro-fabrication techniques have recently shown significant advances, regular-shaped miniature-channel regenerator type can be a good choice as one of parallel-geometry regenerators. A few attempts were reported in literature for the development of new conceptual parallel-geometry regenerators to have superior performance. Ibrahim et al [16] developed a segmented-involute-foil regenerator to minimize the pressure drop effects of cylinder cross-flow and to avoid the large axial conduction losses such as in the case of parallel plates and tube bundles. Their test results showed that higher figure of merit was achieved closer to the ideal parallel-plate regenerators.

On the other hand, Li et al [17] proposed a porous-sheet regenerator with hexagonal-shaped flow channels using dynamic mesh CFD simulation for whole engine. Each flow channel has a side length of 0.4mm and a length of 73mm. They found that, under the same working conditions, the pressure drop for porous-sheet regenerator is lower compared to wire mesh. Optimizing both regenerators under given operating conditions showed that the porous-sheet regenerator had 38%-51% lower entropy generation rate compared to wire mesh, thus contributing to an increase in power and efficiency of the engine. However, experimental testing of porous-sheet regenerator was not reported in his study.

Nam et al [18] developed a parallel wire type regenerator. The friction factor was found to be 20-30% lower than the screen mesh regenerator, but the thermal performance of this new type was poor compared to the screen mesh type due to large axial conduction of parallel wires. The axial conduction losses were further alleviated by the segmentation of the continuous wires but the number of segmentation was limited due to the increased number of housings required to hold the wires. Takizawa et al [19] developed a thin porous-sheet regenerator with small rectangular-shaped flow holes. The effect of this type of regenerators and other two wire screens were tested on an experimental engine stand (NS03T), the results showed that the engine power output was improved by 15% compared to 200M wire sheet.

Isshiki et al [20] investigated experimentally the effect of layered-plate type regenerator on beta-type Stirling engine. They compared the performance of the engine using this type of regenerator to the traditional wire-mesh type. They found that the layered-type had a better performance on the engine compared to the wire-mesh. They justified this to the reduced pressure drop of the layered-type as well as the increases heat transfer due to the

extended area of the layered plates. The engine brake power was achieved in the range of 22 to 91.4 W when heater temperature was varied in the range of 180-330 ˚C. Kato et al [21] proposed a methodology to evaluate the regenerator performance based on experiments. The experimental test facility was similar to that of a 180°-phase angle alpha-type Stirling engine. An electric heater was used to control the hot end temperature while the cold end temperature was controlled by a conditioned air. The LTD engine was tested with polyurethane foam and #18 stainless steel as regenerators. The regenerator effectiveness was calculated in terms of the measured temperature fluctuation between the hot and cold ends. The results showed that regenerator effectiveness of the stainless steel mesh layered parallel to gas flow direction was significantly less in comparison to that of the normal mesh layers while a significant pressure loss was observed for the polyurethane foam when fitted in cylinder/displacer gap.

Based on open literature, there is limited research on micro parallel flow regenerators, therefore in this work, the development of new Stirling engine regenerator based on parallel-geometry configuration using miniature circular channels with diameters of 1.5, 1.0, 0.6, 0.5, 0.4 (mm) were investigated for gamma-type Stirling engine (ST05CNC). A CFD model was developed on a 3D sector of the proposed geometry using transient conjugate heat transfer to determine the fluid flow and heat transfer characteristics of the five configurations for a unidirectional flow. The real geometry of regenerators then is converted into an equivalent porous media so that the engine performance fitted with channels regenerator is evaluated using a full engine CFD model developed by the author in other study [22].

1. Design concept

Fig.1 shows the conceptual design of miniature-channel regenerator which is scaled to the original regenerator dead volume of the engine. The proposed geometry is composed of circular-shaped miniature-channel cutting through the solid matrix with constant diameter. Different diameters are selected for the channels 1.5, 1.0, 0.6, 0.5, 0.4 (mm) so that high surface area density (up to 2600 m^2/m^3) can be achieved, with channels length equals to the regenerator length of 57 mm. The material selected for all samples is stainless steel (SS304), with its properties are listed in **Table 1**.

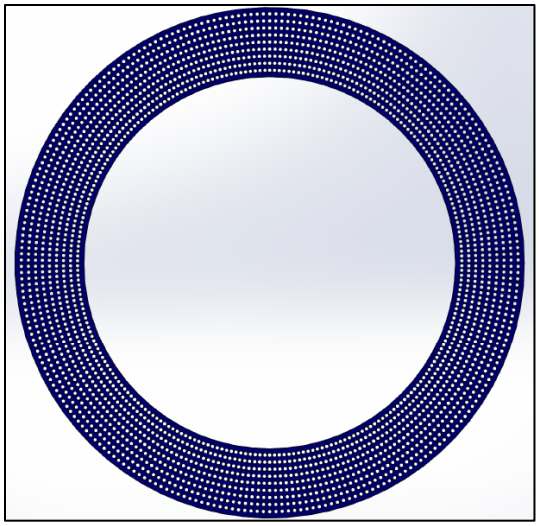

Figure 1: Conceptual design of miniature-channel regenerator

Table 1
Regenerator material thermal properties (SS304L)

Property	**Value**
Density (kg/m^3)	7850
Specific heat capacity (J/kg. K)	475
Thermal conductivity (W/m. K)	16

The circular channels are distributed with radial and angular pitches that satisfy the minimum required thermal penetration depth, which is defined as the distance that heat can diffuse into the solid matrix during single blow time, $t_p = (1/\pi f)$, where f is the frequency of the engine [9]. Since the engine under consideration can operate at speed ranging from 100 to 1000 rpm, then the thermal penetration depth is calculated by Eq. 1 and the results are presented in fig. 2;

$$\delta = \sqrt{(k_s/\pi f \rho C_P)} \quad (1)$$

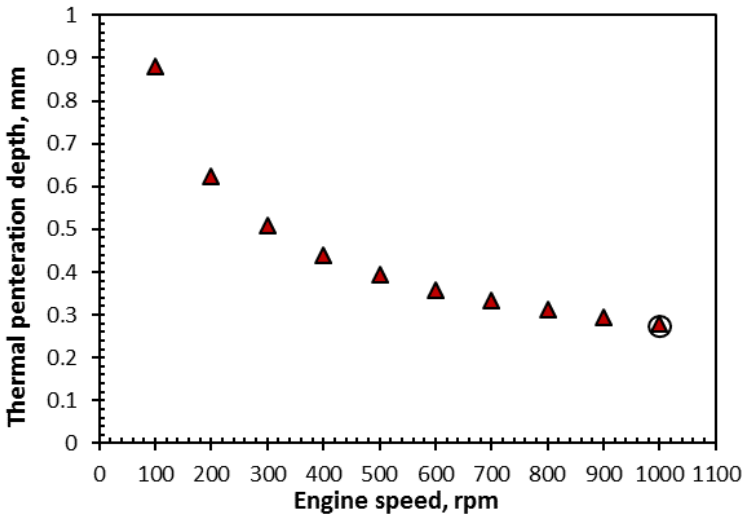

Figure 2: Thermal penetration depth vs. engine speed.

177

178 The radial and angular pitches are not fixed and can be calculated based on the minimum thermal penetration depth
179 of 0.25 obtained at maximum engine speed as shown in fig.2. The geometrical parameters of the regenerator
180 configuration as shown in fig.3 can be calculated from Eq.2 and 3, respectively.

181

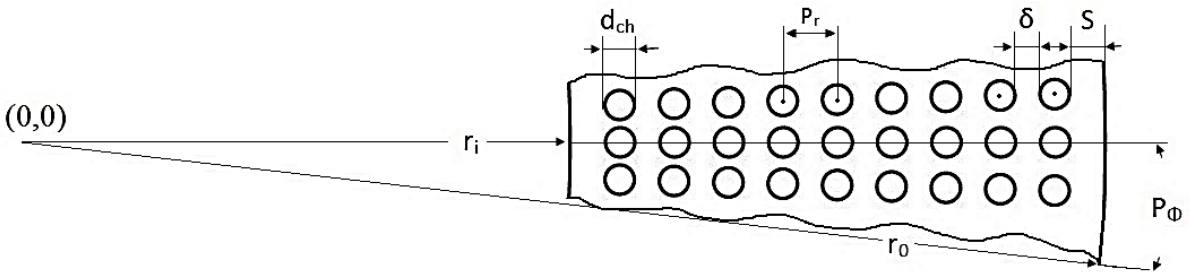

Figure 3: Geometrical parameters of channels regenerator.

182

$$P_r = \delta + d_{ch} \tag{2}$$

183

184 Where the radial pitch is measured from centre to centre of consecutive channels
185
186

$$P_{\emptyset} = 2\sin^{-1}[(d_{ch}/2 + \delta/2)/(d_{ch}/2 + r_i + S)] \quad (3)$$

The angular pitch in (Eq.3) is based on the trigonometric relation exists between the three parameters (d_{ch}, δ and S) at the first row of channels as demonstrated in fig.4.

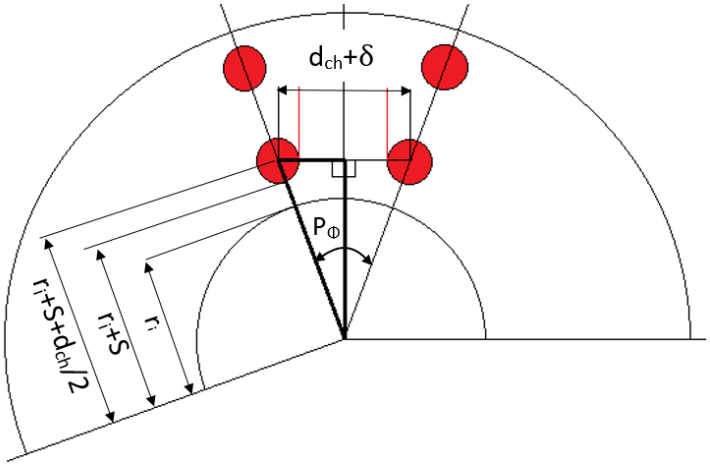

Figure 4: Radial pitch definition in terms of regenerator parameters (not to scale).

The geometrical parameters are calculated for channel diameter ranging from 0.4mm to 1.5 mm and fixed δ value and tabulated in **Table *2***.

Table 2
Regenerators configurations and parameters.

Configuration	**Angular pitch** $P_{\emptyset}$ **(°)**	**Vertical pitch** P_r **(mm)**	**Tubes/sector**	**Tubes/annulus**	**Porosity (%)**
1.5mm	2	1.75	9	180	0.433
1.0mm	1.42	1.25	13	253	0.391
0.6mm	0.9	0.85	20	400	0.343
0.5mm	0.85	0.75	22	500	0.286
0.4mm	0.85	0.65	26	500	0.248

2. CFD Model

Since the regenerator is composed of miniature-channel of circular shape, internal fluid flow and heat transfer are the major physics. COMSOL Multiphysics 5.2 CFD commercial code was used for 3D transient conjugate heat transfer simulation of the regenerator. Prior to the procedure of computational modelling of the regenerator, the testing metrics of CFD computations is a prerequisite to evaluate the accuracy of the current results. Since the flow is developing inside the regenerator channels, a replication of hydrodynamically and thermally developing laminar tube flow was initially conducted.

2.1 Fluid flow and heat transfer in channels

The average friction factor and heat transfer coefficient for a whole tube are enhanced due to the effect of the entrance length [23]. This enhancement is significant for a shorter tube rather than a longer one as the skin shear stress and the heat transfer coefficient are large at the entrance of the tube where the boundary layer thickness is very small. In the developing flow regime, both the velocity and thermal boundary layers are growing in the flow direction where the velocity and temperature profile are locally varying up to a certain distance downstream of the tube. The flow is then said to be *fully developed*, and the *parabolic profile* is obtained for laminar flow in a circular tube. In the entrance region, the boundary layer of the developing flow needs to be captured by the computational grid for accurate solutions.

The hydrodynamic entry length, for laminar flow (Re < 2300), can be expressed in the form [24]

$$\left(\frac{x_{fd,h}}{D}\right) \approx 0.05Re \tag{4}$$

In the fully developed region, the pressure gradient is constant and the velocity profile is recalled from [24] as

$$u(r) = 2u_m \left[1 - \left(\frac{r}{R}\right)^2\right] \tag{5}$$

It follows that the ratio of the maximum and averages velocities in the fully developed region

$$u_{max} = 2u_m \tag{6}$$

According to Shah and London [25], The friction factor – Reynolds number product (fRe) for laminar flow is

$$fRe = 16 \tag{7}$$

If tube surface is maintained at either uniform temperature or uniform heat flux, conduction and convection heat transfer occurs and the *boundary layer* begins to develop thermally until the fully developed temperature profile is reached.

The *thermal entry length* for laminar flow can be expressed as

$$\left(\frac{x_{fd,t}}{D}\right) \approx 0.05 ReP_r \tag{8}$$

When a tube flow is considered, heat transfer occurs by conduction when the fluid layers are stationary near the wall and by forced convection when the fluid flowing through the tube. The ratio of the convective heat flux to the conductive heat flux is referred to, Nusselt number (*Nu*) and it is defined as

$$Nu = \frac{h_x D_h}{k_f} \tag{9}$$

In a horizontal tube, under constant wall temperature boundary condition, the thermal characteristics of the flow is defined by the fluid bulk temperature, heat transfer coefficient, heat flux, and the Nusselt number. The fluid bulk temperature, is obtained in terms of the true energy advection over an arbitrary cross section of the pipe.

Therefore, T_m is defined by

$$T_{m,x} = \frac{\int \rho u C_p T \, dA_c}{m C_p} \tag{10}$$

The other important parameter is the heat transfer coefficient which is defined by

$$h_x = \frac{q''_x}{(T_w - T_{m,x)}} \tag{11}$$

Where

$$q''_x = k_f \left[\left(\frac{\partial T}{\partial r}\right)_{w,m}\right]_x \tag{12}$$

Where $\left(\frac{\partial T}{\partial r}\right)_{w,m}$ represents the peripheral average temperature gradient at wall.

As a special case for a fully developed laminar flow in case of constant wall temperature in a circular tube, *the rate of net energy transfer to the control volume by mass flow is equal to the net rate of heat conduction in the radial direction,* leads to the common value of Nusselt number,

$$Nu = 3.66 \tag{13}$$

2.2 Governing equations and solution methodology

For steady-state incompressible viscous flow, the Navier-Stokes equations which describe the velocity, pressure, temperature, and density of a moving fluid based on conservation of mass, momentum and energy, for the computational domain can be written as;

$$\rho \nabla . (\boldsymbol{u}) = 0 \tag{14}$$

$$\rho(\boldsymbol{u}.\nabla)\boldsymbol{u} = \nabla.[-p\boldsymbol{I} + \mu\ (\nabla\boldsymbol{u} + (\nabla\boldsymbol{u})^T) + \boldsymbol{F} \quad (15)$$

$$\rho C_p\, \boldsymbol{u}.\nabla T + \nabla.k\nabla T = Q \quad (16)$$

These coupled differential equations are solved by finite element-based CFD software (Comsol multiphysics). In order to carry out the simulation, a prerequisite of mesh sensitivity analysis is initialized to ensure that the numerical solutions obtained are grid-independent. Using symmetry can provide faster solution in which a quarter of the current 3D tube is selected as the computational domain as shown in fig.5. The tube has (1 in) diameter and (12 in) length which is subdivided into six sections in order to calculate the developing Nusselt number downstream of the inlet.

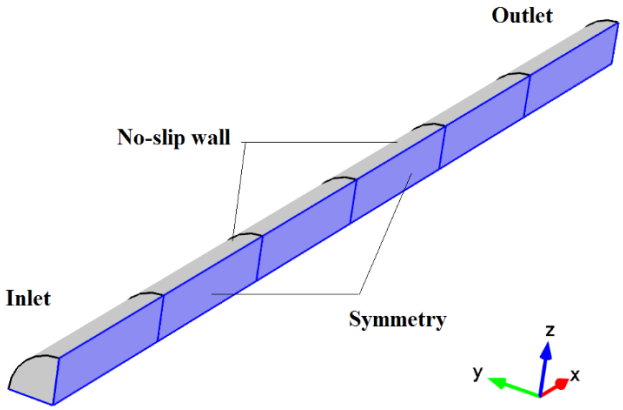

Figure 5: Computational domain of the tube.

The boundary conditions are applied as follows;

- Constant wall temperature of 310 K is applied on the outer walls of the pipe.
- Uniform inlet velocity (based on Re =100) at constant temperature of 300 K is applied at the tube inlet.
- Outlet pressure of 101,325 kPa with no back flow is applied at the tube outlet.
- Free-slip symmetry walls with zero normal velocity components and normal gradients of all velocity components.

The meshing sequence is varied from coarse to extra-fine size as shown in fig.6. This will define mesh size that gives an accurate solution with less computational time required to perform the CFD simulation. The face elements then are swept over the length of the tube based on each sequence. **Table *3*** summarises the details of each meshing sequence and the obtained solution of Nusselt number.

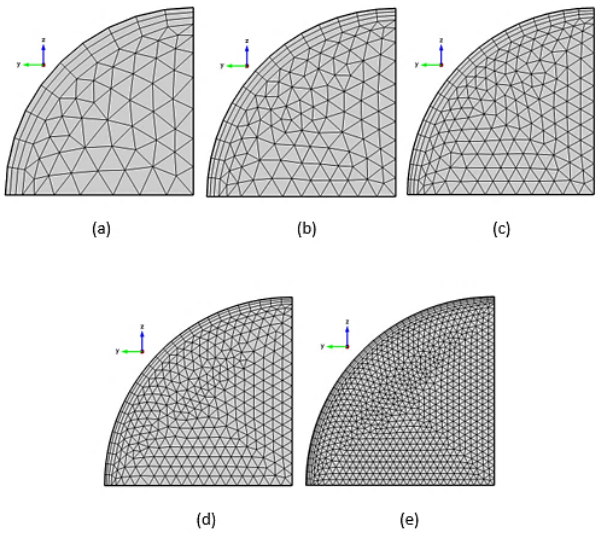

Figure 6: Meshing sequence, a) coarse, b) normal, c) fine, d) finer, e) extra-fine.

Table 3
Mesh sequence and CFD results

Mesh sequence	No of elements	Mesh quality	Growth rate	Nu
Coarse	19908	0.6558	1.344	6.2728
Normal	57354	0.7324	1.317	6.1937
Fine	103840	0.7747	1.269	6.1387
Finer	283920	0.8139	1.229	6.0173
Extra-fine	1,116,220	0.8614	1.189	5.9435

From the data obtained in **Table *3***, finer meshing sequence can be selected for the investigation as the change of Nusselt number is less than 1.3% compared to the extra-fine sequence. The velocity and temperature contours are plotted in fig. 7 and 8. It is clearly shown that both hydrodynamic and thermal boundary layers are developing downstream of the tube inlet. A first check to carry out was to calculate the ratio of the maximum velocity

magnitude to the average velocity magnitude at the end of the pipe and the product of Reynolds number with friction factor. It is recalled that from the analytical solutions available in literature, Eq.6 that this ratio is double since the pressure gradient is constant in the fully developed region. Since the entry length required for this tube is calculated from Eq.7 equals 12.7 cm which means that the flow should be hydrodynamically fully developed at the end of the pipe and the product of Reynolds number with friction factor equals to 16. The comparison made in **Table *4*** has shown good agreement with the available analytical solution.

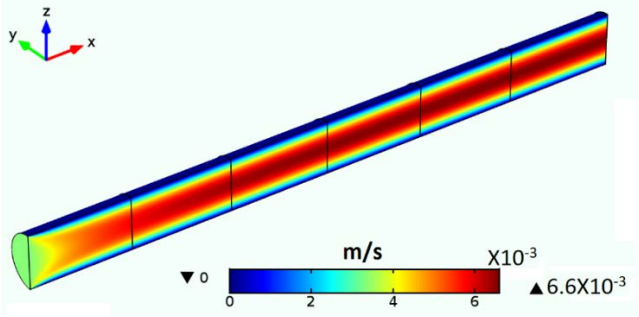

Figure 7: Velocity contours along the tube.

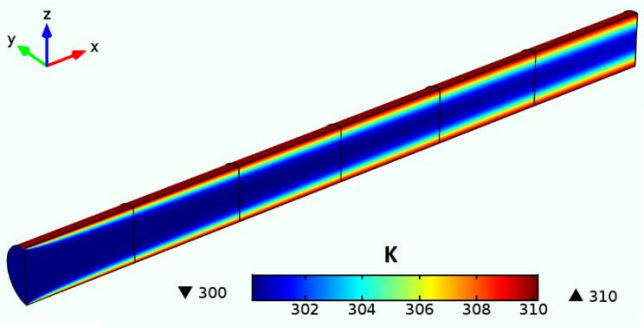

Figure 8: Temperature contours along the tube.

Table 4

Comparison between CFD results and analytical data for fully developed tube flow.

Parameter	CFD	Analytical solution [24]
$\mathbf{u_{max}/u_{mean}}$	1.97	2
fRe	17.4	16

In order to validate the CFD results of the obtained Nu number in the case of developing flow, [26] was selected for the comparison which is recommended for a combined entry length under constant wall boundary condition. The results of Nusselt number was compared to Hausen's correlation in fig.9. As shown, both results are reasonably matched with a deviation in the range of 5-11%.

$$\overline{Nu_D} = 3.66 + \left[\frac{0.0668 G_{Z_D}}{1 + 0.04 G_{Z_D}^{\frac{2}{3}}}\right] \quad (17)$$

Where G_{Z_D} is a dimensionless parameter defined as,

$$G_{Z_D} = \left(\frac{D}{x}\right).R_e.P_r \quad (18)$$

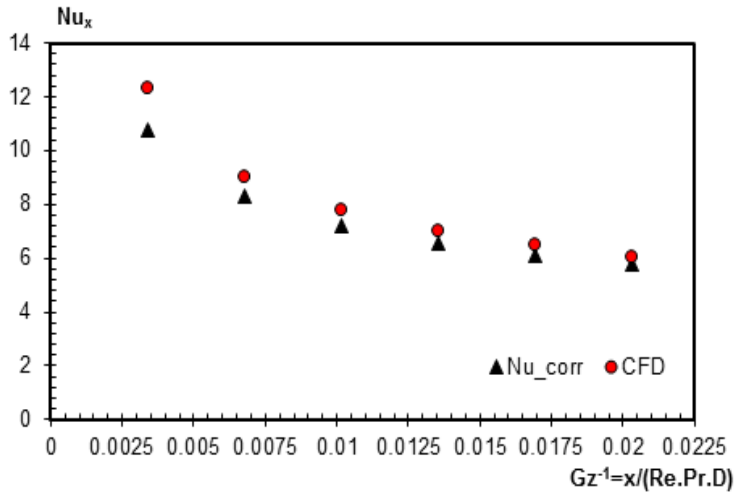

Figure 9: Nusselt number for laminar developing pipe flow.

3. Regenerator modelling

From a microscopic point of view, it is not feasible to model the regenerator as a whole as depicted in fig.1. Therefore, more simplification is realized when a certain sector is repeated in the angular-direction with a certain pitch ($P_\emptyset$), it resembles the flow through regenerator annulus. The depth of the sector is taken as whole regenerator length. Inlet velocity at constant temperature of 650 °C is specified at channels inlet, while pressure outlet at 10 bar

with outflow boundary is prescribed at the outlet. These boundary conditions are similar to the actual operating conditions of the engine during single hot blow period. The maximum inlet velocity to the sector channels, is varied according to the engine frequency and displacer swept volume, and is calculated by;

$$v_{max} = \pi . f . VSWE \, / A_f \tag{19}$$

The outer walls and the inner wall of the sector (except the channels) are adiabatic and the reference pressure is the charge pressure of the engine. Transient conjugate heat transfer simulations based on compressible laminar flow were carried out for all configurations following the same procedure of meshing sequence described in section 3.

4. Engine description

The engine under study is a gamma-type that was first designed by Dieter Viebach in 1992 in Germany to promote microgeneration with biomass fuels and since then was opened for research development [27]. The engine, shown in fig. 10, consists of power and displacer pistons with 90° phase angle, and three heat exchangers (heater, cooler and regenerator) and a connecting pipe. The expansion and compression spaces are connected via a 30-mm concentric-cooled pipe. Meanwhile, the engine is heated up to 650 °C by an external electric heating unit and cooled by a circuit of cooling water normally at 15°C. The geometrical and operational parameters of the engine are listed in **Table *5***.

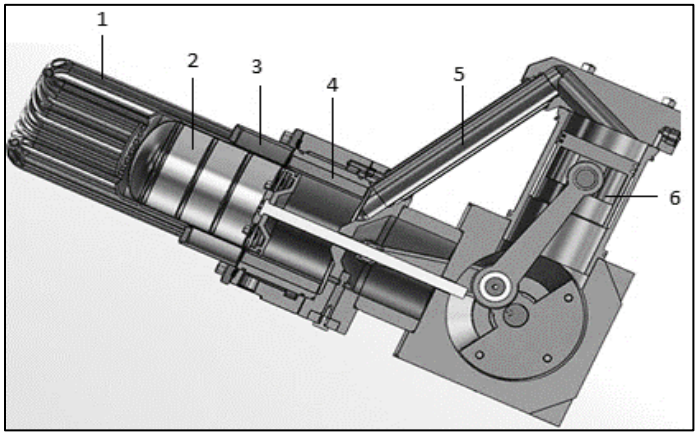

Figure 10: Engine components: 1-Heater, 2-Displacer piston, 3-Regenerator, 4-Cooler, 5-Connecting pipe, 6-Power piston.

Table 5
Engine's geometrical and operational parameters.

Parameter	Value/description
Nominal rotational speed (rpm)	500
Stroke (mm)	75
Power piston bore (mm)	85
Displacer piston bore (mm)	96
Charge pressure (bar)	10
Working gas	N_2
Heater type	Tubular
Cooler type	Finned
Regenerator type	Annular/Random fibre
Wire diameter (Micron)	31
Porosity	0.9
Hot source temperature (°C)	650
Inlet water temperature (°C)	15
Water flow rate (L/min)	3.5
Water cooling power (kW)	2.3
Compression ratio	1.3

A full CFD model of the engine developed by the author in a previous study [22] will be used to investigate the effect of channels regenerator on engine performance in section 5. The model was based on a realistic Local Thermal Non-Equilibrium (LTNE) approach for porous domains in the engine (cooler and regenerator), compressible laminar Non-Isothermal flow for nonporous domains and moving boundaries of the pistons. The model results showed an acceptable degree of accuracy of 9% and 5%, respectively when comparing with experimental results in predicting the indicated and cooling powers at different heating temperatures.

Results and discussion

A sample of the temperature contours of 1.5 mm channels regenerator at two extreme engine speeds were presented in figs. (11-12). Most of the heat is transferring in the radial direction depending on the gas inlet velocity through the channels. As the inlet velocity to the regenerator sector increases from 100rpm (fig.11) to 1000rpm (fig.12), more energy is transferred to the solid matrix due to the forced convection giving a rise to the average solid temperature of the matrix. As can be seen that the minimum temperature of the matrix at 100rpm is 500 °C compared to 865 C° at 1000 rpm.

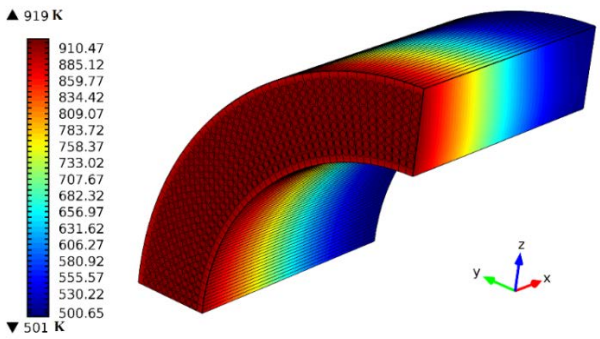

Figure 11: Temperature contours for 1.5mm channels regenerator at speed of 100 rpm and time of 30s.

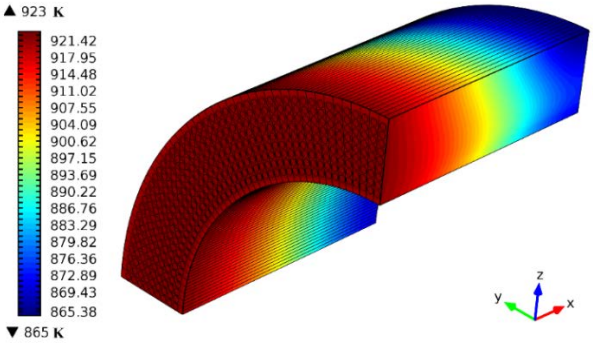

Figure 12: Temperature contours for 1.5mm channels regenerator at speed of 1000 rpm and time of 30s.

366

367

368 The fluid flow and heat transfer characteristics were obtained from CFD simulations for each configuration and are
369 plotted in fig.13-15. As can be seen that data of pressure loss (fig.13) shows almost linear trends with gas inlet
370 velocity for all regenerator configurations. The inertial loss part is not significant in the channels due to the absence
371 of flow separation and vortices. The highest pressure loss is observed for 0.4mm channels regenerator.

372

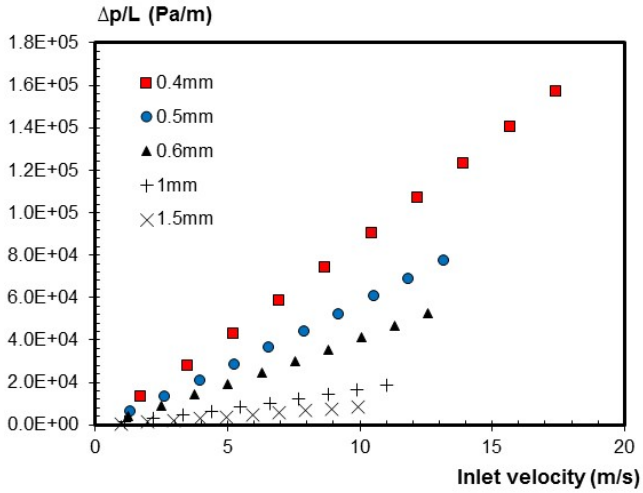

Figure 13: Pressure loss per unit length vs. gas inlet velocity to the regenerator for different channels regenerators.

373

374 The simulation results for friction factor and Nusselt number were plotted in fig.14-15. The average friction factor
375 shows a decreasing trend with increasing Reynolds number for all configuration, in which the friction factor
376 correlations are close to Darcy friction factor for laminar flow.
377

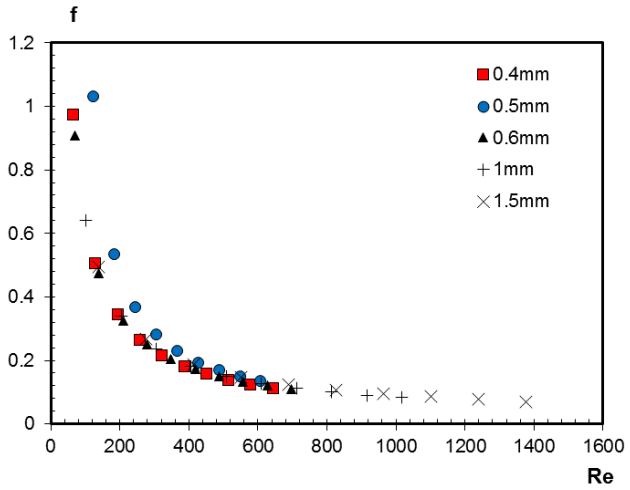

Figure 14: Darcy friction factor vs. Reynolds number for different channels regenerators.

378

379 Fig.15 shows that the average Nusselt number increases with the fluid flow velocity. This result is natural and it
380 agrees with the principles of forced convection. For larger diameter channels, higher values of Nusselt number is
381 depicted in fig.15 due to the higher values of hydraulic diameters. However, the small channels regenerators indicate
382 faster thermal response at a small range of Reynolds number (100 to 700) compared to larger diameter channels
383 (100 to 1400). In terms of heat transfer coefficient, larger diameter channels experience low heat transfer
384 coefficients due to the limited heat transfer surface area.

385

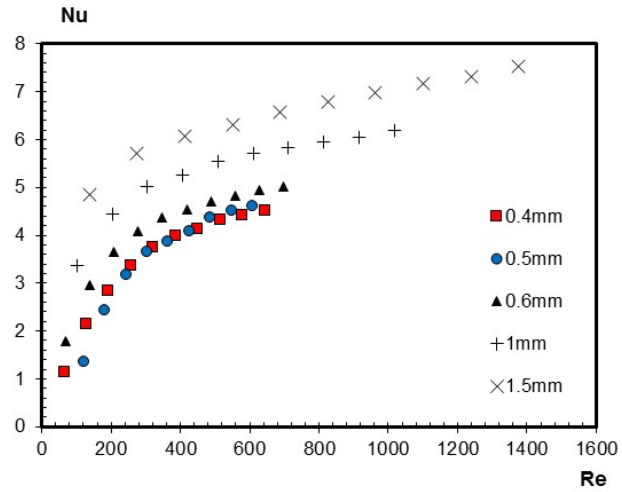

Figure 15: Nusselt number vs. Reynolds number for different channels regenerators.

386

387 The pressure drop-velocity data of each regenerator was fitted to Forchheimer-Darcy equation (Eq.20) using the
388 least square method in order to obtain the equivalent porous media parameters (porosity, Forchheimer drag
389 coefficient and permeability).

$$\frac{\nabla p}{L} = \frac{\mu}{K}\, u + \beta_F\, u^2 \tag{20}$$

390

391 All simulation results such as Nusselt number correlations and porous media parameters were tabulated in ***Table 6***.
392 The specific solid surface area is used in porous media modelling to quantify the non-equilibrium source term when
393 solving both energy equations of the gas and solid phases. It is defined as the ratio of the matrix surface area
394 exposed to the gas to the volume of the matrix and can be calculated in terms of porosity (ε) and hydraulic
395 diameter (d_h) from [22]

$$a_{fs} = \frac{4\varepsilon}{D_h} \tag{21}$$

396

This data of each configuration will be used as input parameters to the engine CFD model to evaluate the performance of the engine with each configuration. This will include evaluating the indicated and cooling powers of the engine for the comparison.

Table 6
Equivalent porous media characteristics of the three proposed regenerators.

Regenerator type	Permeability, K (m^2)	Forchheimer drag coefficient, β_F (kg/m^4)	Nusselt number	Specific surface area (1/m)
0.4mm	4.95E-09	61.375	$0.124Re^{0.5747}$	2475
0.5mm	7.73E-09	59	$0.195Re^{0.5126}$	2617
0.6mm	1.1E-08	49.2	$0.34Re^{0.4249}$	2284
1.0mm	3E-08	32.925	$1.143Re^{0.2488}$	1565
1.5mm	6..26E-08	23	$2.018Re^{0.1812}$	1156

The variation of matrix temperature versus the length of regenerator at the end of the 5th cycle for 0.5 mm channels regenerator is depicted in fig.16. It is worth noting how the temperature variation remarkedly deviates from the well-known linear trend with the appearance of large curvature during the cold and hot blow times. This curvature caused a considerable exchange of energy between the gas and the matrix. The axial conduction loss is a key mechanism that occurs in channel regenerators and tends to lower the NTU of the matrix due to the large temperature gradient between the gas and the solid. This can be more illustrated in fig.17 when the solid and gas temperatures are plotted over the cycle.

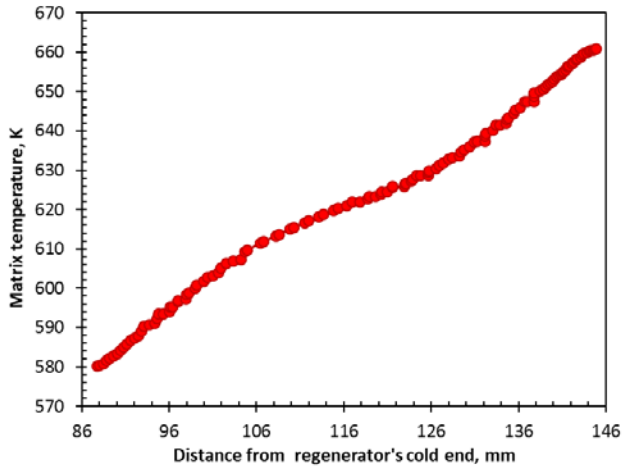

Figure 16: Axial temperature variation of regenerator matrix for the 0.5 mm channels regenerator.

412

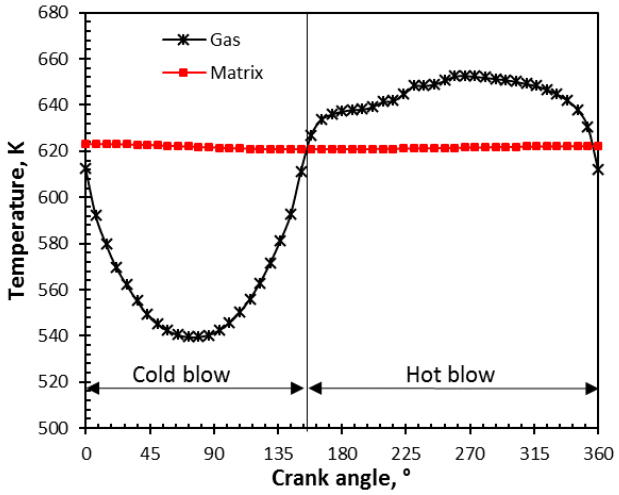

Figure 17: Gas and matrix temperatures variation in the regenerator over one cycle.

413

414 An amplitude of several degrees was observed between the gas and matrix temperatures during the cycle. As can be
415 seen that the process of heat regeneration occurs due to heat release and storage in the matrix. During cold blow
416 period, the gas enters the regenerator with a temperature lower than the matrix temperature. Meanwhile, in the hot
417 blow period, the gas temperature becomes higher than the matrix one.

418

419 Fig.18 shows the engine indicated power for channels regenerators and random fibre at a heating temperature of 650
420 °C. As depicted, the indicated power of 0.5mm regenerator is 4% lower than that of the random fibre regenerator.
421 As the channels diameter increases, the indicated power deteriorates reaching a reduction of 31% for 1.5mm
422 regenerator compared to that of random fibre. Although pressure drop of channels regenerator is significantly lower
423 than that of conventional regenerators, the performance of the engine is governed by the heat transfer characteristics
424 of the regenerator.

425
426
427

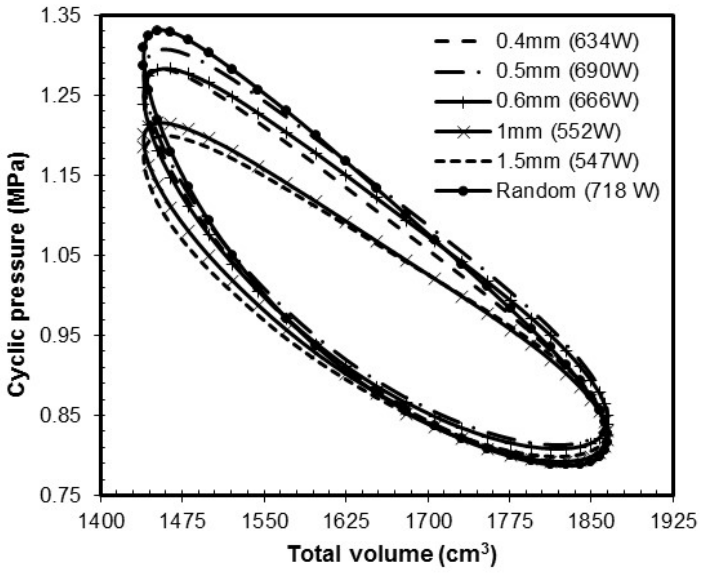

Figure 18 Indicated PV diagrams for channels regenerator and random fibre.

Fig.19 shows a comparison of the heat rejected from engine's cooler for channels regenerator and random fibre where the maximum heat rejected from the engine is observed for 1.5mm channel regenerator which is 17% higher than that of the random fibre. One important factor of regenerator performance is the specific surface area exposed to the working gas. Since heat transfer resistance between the gas and the solid is much higher than the resistance inside the regenerator. Therefore, transferring the heat from the gas to the regenerator can be enhanced by increasing the specific surface area.

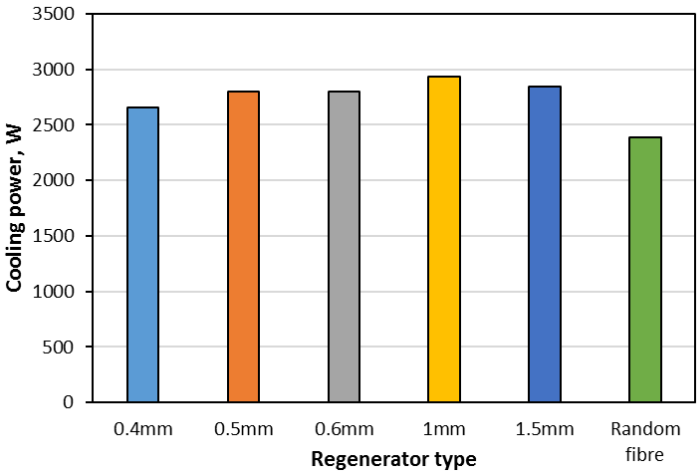

Figure 19: Cooling power for channels regenerator and random fibre.

A closer comparison of the solid specific areas between the random fibre and channel regenerators showed that the surface area of all channel regenerators is limited which is lower than that of random fibre. However, the volumetric heat capacity of the channel regenerator is significantly higher than that of random fibre due to a lower porosity. The ineffectiveness in channels regenerators was their excessive conduction loss due to high longitudinal thermal conductivity. Therefore, the regenerator's NTU is reduced due to the reduction of the temperature difference between the working gas and matrix.

However, the ineffectiveness of channels regenerators can be alleviated by optimizing the matrix material and the segmentation of the whole regenerator. The thermal performance of the regenerator is governed by the choice of its material. A material with good heat capacity allows to absorb/release maximum energy to/from the working gas and a material with lower thermal conductivity reduces conduction losses. Different materials such as Stainless steel, Monel 400, ceramic (ZrO2), copper and aluminium with different thermal properties, were investigated using the engine full CFD model. The thermal properties of those material are listed in **Table *7***.

Table 7
Material thermal properties of regenerator matrix [14].

Properties	**Stainless steel (304L)**	**Copper**	**Aluminium**	**Monel 400**	**Ceramic (ZrO2)**
Density (kg m^{-3})	7850	8920	2700	8800	6050
Thermal capacity (J kg^{-1} K^{-1})	475	385	902	430	460
Thermal conductivity (J kg^{-1} K^{-1})	26*	390	237	22	3

*recommended for Stirling engine environment based on oscillatory flow condition [28]

Monel 400 and Stainless steel have the highest volumetric heat capacity (material density times the specific heat capacity) among those materials and lower thermal conductivity. Therefore, it is expected that those two materials will show better performance compared to copper and aluminium with higher thermal conductivities. In order to

investigate the effect of those materials on engine performance, the maximum heater temperature of the engine was maintained at 500 °C to avoid approaching the melting point of aluminium. As depicted in fig.20, higher indicated power was obtained using Monel 400 and Stainless steel, while copper has the lowest indicated power. In terms of the cooling power rejected from the engine, ceramic (ZrO2) and Monel 400 had the lowest cooling power while copper had the highest. This proves that the best regenerator material should have a reasonable volumetric heat capacity and a lower thermal conductivity.

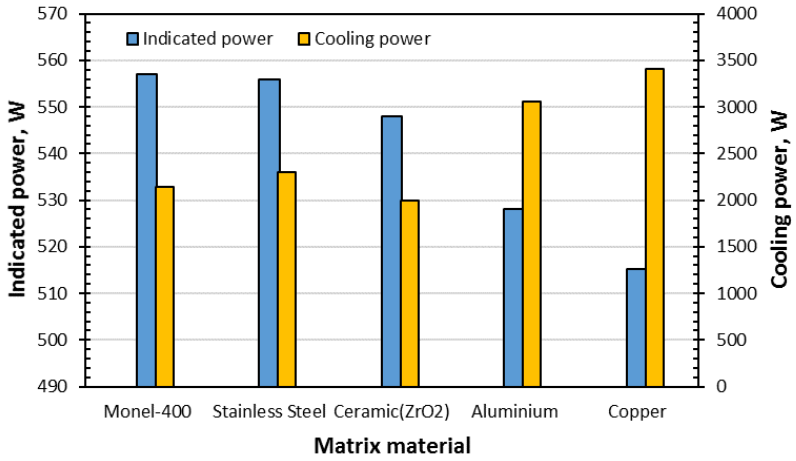

Figure 20: Indicated and cooling powers for different matrix materials.

Segmentation of the regenerator adds thermal contact resistance to each consecutive sheets so that the axial conduction loss is minimized due the interruption of the solid continuity. Similar behaviour was observed by authors [18, 29] where they conducted an experimental study to find the optimum number of segmentations for parallel wire regenerator. The theoretical investigation of segmentation of a parallel geometry regenerator was not reported in literature due to the lack of defining thermal contact characteristics that resembles the real cutting properties of the sheets such as surface roughness (height and slope), hardness of the material, contact pressure and the gap conductance. Therefore, the next phase of this design will be based on regenerator segmentation and experimental investigation of heat transfer and fluid flow characteristics of the different configurations of channel regenerators.

5. Conclusion

Potentiality of new Stirling regenerator as one of parallel-geometry regenerators was investigated using CFD simulations. Circular miniature-channels with different diameters in the range of (0.4 to 1.5mm) were adopted in this study. The metrics of CFD results was initially set up to replicate fluid flow and heat transfer characteristic for a developing laminar pipe flow. A transient conjugate heat transfer simulations were performed on a 3D regenerator sector to obtain heat transfer and fluid flow characteristics for all configuration of channels regenerators. The obtained data was converted into equivalent porous media characteristics and then was utilized for full engine CFD simulations. The results showed that small channels regenerators (0.5mm) can have good potential to generate power as random fibre. It was found that the higher cooling power of the engine using channels regenerators is posed by the axial conduction loss. The matrix material of channel regenerator can have strong impact on regenerator performance. The results showed that using materials such as ceramic (ZrO2) and Monel 400 can alleviate the axial conduction loss due to the low thermal conductivity and enhance the engine performance. A further 3D CFD study on an oscillatory pipe flow will follow this initial design with an experimental verification of regenerator segmentations to further optimize the channels regenerators performance.

Acknowledgments

The authors gratefully acknowledge the funding from the (EPSRC) 'Engineering and Physical Sciences Research Council' under Grant NO. EP/LO17725/1 for enabling the purchase of the Stirling engine used in this research. Also, the authors acknowledge the Ph.D. sponsorship received from University of Benghazi and the Libyan Ministry of Higher Education and Scientific Research.

References

1. Goswami, D.Y. and F. Kreith, *Handbook of energy efficiency and renewable energy*. 2007: Crc Press.

2. Ibrahim, M.B. and R.C. Tew Jr, *Stirling convertor regenerators.* 2011: CRC Press.

3. Organ, A.J., *The regenerator and the Stirling engine*. 1997: wiley.

4. Walker, G., *Stirling-cycle machines*. 1973: Oxford University Press.

5. Organ, A.J., *Thermodynamics and gas dynamics of the Stirling cycle machine*. 1992: Cambridge University Press.

6. Radebaugh, R. and B. Louie. *A simple, first step to the optimization of regenerator geometry*. in *In its Proc. of the 3rd Cryocooler Conf. p 177-198 (SEE N86-11367 02-31)*. 1985.

7. Martini, W.R., *Stirling engine design manual*. 1978: US Department of Energy, Office of Conservation and Solar Applications, Division of Transportation Energy Conservation.

8. Martaj, N.G., Lavinia Rochelle, Pierre, *Thermodynamic study of a low temperature difference Stirling engine at steady state operation.* International Journal of Thermodynamics, 2007. **10**(4): p. 165-176.

9. Shendage, D., S. Kedare, and S. Bapat. *Investigations on performance of Stirling engine regenerator matrix*. in *ASME/JSME 2011 8th Thermal Engineering Joint Conference*. 2011. American Society of Mechanical Engineers.

10. Mahkamov, K., *Design improvements to a biomass Stirling engine using mathematical analysis and 3D CFD modeling.* Journal of Energy Resources Technology, 2006. **128**(3): p. 203-215.

11. Della Torre, A., et al. *CFD MODELLING OF A BETA-TYPE STIRLING MACHINE*. in *5th European Conference on Computational Mechanics (ECCM V), Barcelona*. 2014.

12. Costa, S., et al., *Numerical study of the heat transfer in wound woven wire matrix of a Stirling regenerator.* Energy Conversion and Management, 2014. **79**: p. 255-264.

13. Chen, W.-L., K.-L. Wong, and H.-E. Chen, *An experimental study on the performance of the moving regenerator for a γ-type twin power piston Stirling engine.* Energy Conversion and Management, 2014. **77**: p. 118-128.

14. Gheith, R., F. Aloui, and S.B. Nasrallah, *Determination of adequate regenerator for a Gamma-type Stirling engine.* Applied Energy, 2015. **139**: p. 272-280.

15. Gheith, R., F. Aloui, and S.B. Nasrallah, *Study of temperature distribution in a Stirling engine regenerator.* Energy Conversion and Management, 2014. **88**: p. 962-972.

16. Ibrahim, M.B., et al., *A Microfabricated Segmented-Involute-Foil Regenerator for Enhancing Reliability and Performance of Stirling Engines: Phase II Final Report for the Radioisotope Power Conversion Technology NRA Contract NAS3-03124.* 2007.

17. Li, Z., et al., *Analysis of a high performance model Stirling engine with compact porous-sheets heat exchangers.* Energy, 2014. **64**: p. 31-43.

18. Nam, K. and S. Jeong, *Development of parallel wire regenerator for cryocoolers.* Cryogenics, 2006. **46**(4): p. 278-287.

19. Takizawa, H., et al. *Performance of new matrix for Stirling engine regenerator*. in *Energy Conversion Engineering Conference, 2002. IECEC'02. 2002 37th Intersociety*. 2004. IEEE.

20. Isshiki, S., et al., *The Experimental Study of Atmospheric Stirling Engines Using Pin-Fin Arrays' Heat Exchangers.* Journal of Power and Energy Systems, 2008. **2**(5): p. 1198-1208.

21. Kato, Y. and K. Baba, *Empirical estimation of regenerator efficiency for a low temperature differential Stirling engine.* Renewable Energy, 2014. **62**: p. 285-292.

22. Alfarawi, S., R. AL-Dadah, and S. Mahmoud, *Influence of phase angle and dead volume on gamma-type Stirling engine power using CFD simulation.* Energy Conversion and Management, 2016. **124**: p. 130-140.

23. Yunus, C. and J. Afshin, *Heat and Mass Transfer: Fundamentals and Applications*. 2011, Tata McGraw-Hill, New Delhi, India.

24. Kakaç, S., R.K. Shah, and W. Aung, *Handbook of single-phase convective heat transfer*. 1987: Wiley New York et al.

25. Shah, R.K. and A.L. London, *Laminar flow forced convection in ducts: a source book for compact heat exchanger analytical data*. 2014: Academic press.

26. Hausen, H., *Darstellung des Warmeuberganges in Rohren durch verallgemeinerte Potenzbeziehungen.* Z. VDI Beih. Verfahrenstech, 1943. **4**: p. 91-98.

27. Ve-ingenieure, *ST05-CNC Stirling engine*. 2016: http://ve-ingenieure.de/projekt_st05g_cnc_engl.html.

28. Urieli, I. and D.M. Berchowitz, *Stirling cycle engine analysis*. 1984: Taylor & Francis.

29. Barari, F., *Metal foam regenerators; heat transfer and pressure drop in porous metals*. 2014, Ph.D, University of Sheffield.